Smart Structures and Systems, Vol. 1, No. 2 (2005) 141-158
DOI: http://dx.doi.org/10.12989/sss.2005.1.2.141

Distributed crack sensors featuring unique memory capability for post-earthquake condition assessment of RC structures

Genda Chen† and Ryan McDaniel‡

Department of Civil, Architectural & Environmental Engineering, University of Missouri-Rolla, Rolla, Missouri, USA

Shishuang Sun‡†, David Pommerenke‡‡ and James Drewniak‡‡†

Department of Electrical and Computer Engineering, University of Missouri-Rolla, Rolla, Missouri, USA

(Received April 8, 2004, Accepted March 24, 2005)

Abstract. A new design of distributed crack sensors based on the topological change of transmission line cables is presented for the condition assessment of reinforced concrete (RC) structures during and immediately after an earthquake event. This study is primarily focused on the performance of cable sensors under dynamic loading, particularly a feature that allows for some "memory" of the crack history of an RC member. This feature enables the post-earthquake condition assessment of structural members such as RC columns, in which the earthquake-induced cracks are closed immediately after an earthquake event due to gravity loads, and are visually undetectable. Factors affecting the onset of the feature were investigated experimentally with small-scale RC beams under cyclic loading. Test results indicated that both crack width and the number of loading cycles were instrumental in the onset of the memory feature of cable sensors. Practical issues related to dynamic acquisition with the sensors are discussed. The sensors were proven to be fatigue resistant from shake table tests of RC columns. The sensors continued to show useful performance after the columns can no longer support additional loads.

Keywords: nondestructive testing; sensors; crack detection and localization; shake table tests; post-disaster condition assessment.

1. Introduction

During post-earthquake condition assessments, prompt evaluation of damage level and structural integrity of both essential and non-essential structures is vital to the continuation of emergency services as well as to the routine operation of civilian services and normal social function. In the case of RC structures, the identification of problematic cracks in load-bearing members is one of the most important factors in evaluating the severity of structural damage. Often times, the cracks are hidden by

†Associate Professor, Corresponding Author, E-mail: gchen@umr.edu
‡Research Assistant, rdmk4@umr.edu
‡†Research Assistant, sspmc@umr.edu
‡‡Associate Professor, Pommerenke@umr.edu
‡‡†Professor, drewniak@umr.edu

architectural furnishings, difficult to detect or completely undetectable by visual inspection because gravity loading has closed them after a catastrophic event.

Cracks in RC members may lead to structural degradation due to reinforcement corrosion associated with the water leakage and chloride invasion, particularly in maritime facilities. Cracks may also significantly increase the deflection of a structure that hinders its functionality under service loading. The minimum crack width that has structural implications is approximately 0.33 mm for interior exposure or 0.41 mm for exterior exposure (Nawy 2003). In the case of nuclear reactors or other solid waste treatment plants, however, this limit would be much smaller in order to prevent any leakage of hazardous materials. On the other hand, a cracked structure can often support additional loading before it becomes unstable. Therefore, the crack width of engineering significance covers a wide range, making it challenging to detect cracks with embedded sensors.

Since the 1970s, Electrical Time Domain Reflectometry (ETDR) has been applied to detect moisture and measure displacements in geotechnical facilities. Most of the recent developments in these applications were summarized in a state-of-the-art review by Benson and Bosscher (1999), and in the book by O'Connor and Dowding (1999). Use of ETDR for the purpose of damage detection of RC structures, however, has a more recent origin. Only a few attempts have been made to detect cracks in RC structures. After a number of laboratory tests on small-scale beams with embedded cable sensors (Su 1997, Lin, *et al*. 1998), it was understood that a commercial cable as a sensor is insensitive to the axial deformation applied to it in structural applications. To improve sensitivity, a prototype cable was designed and fabricated by Lin, *et al.* (2000), in which rubber was used as an insulator of the cable instead of polyethylene or Teflon materials that are used in commercial cables. Rubber was selected due to its low stiffness so that a large deformation is expected to occur when the cable is subjected to an external load. However, a coaxial cable embedded in concrete is subjected to a strain action.

To significantly improve the sensitivity of commercial cables for structural health monitoring, a novel concept of cable design was proposed by Chen, *et al*. (2004). Several prototype sensors were fabricated and tested under static loading when embedded in small-scale RC beams. Test results indicated the superior performance of the sensors in locating and detecting cracks of RC beams. They were also installed into a full-scale RC girder for crack monitoring as well as for understanding of possible signal loss along the sensors (Chen, *et al*. 2003). The sensitivity, spatial resolution, and signal loss issues associated with the crack sensors were further investigated both analytically and numerically (Sun, *et al*. 2004). Shake table tests of RC columns with embedded sensors, however, indicated that the sensors were much less effective under dynamic loads. Most of the recent developments of the novel cable sensors are summarized in Chen (2004).

A new design of cable sensors is introduced in this paper to enhance the performance of the sensors, particularly under dynamic loading. The sensors were embedded in 1/5-scale RC columns. During the tests it was observed that the sensors had the capability of recording the crack history of the columns. When the tests had been completed and the cracks in the column faces were closed due to gravity loads, the signal reflection along the sensors continued to show the location of the cracks that had propagated during testing. To investigate this feature, sensors were placed in six small-scale RC beams and tested statically and cyclically in order to better understand the parameters affecting the feature of the distributed crack sensors. Practical issues are also addressed in this paper, which are related to the ruggedness and fatigue of the sensors, as well as the dynamic acquisition with the sensors.

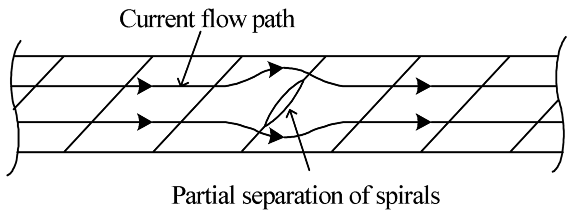

Fig. 1 Current flow in the outer conductor of a coaxial cable made with a spirally wrapped outer conductor with a separation

2. Distributed crack sensor mechanism

The distributed crack sensors are actually coaxial cables. In the previous study by Chen, *et al.* (2004), each sensor consists of a solid inner conductor, a spirally-wrapped copper-tape outer conductor, and a rubber tube in between the conductors as dielectric, which is referred to as rubber-sensor for the remaining presentation of this paper. It differs from a commercial coaxial cable in that the topology of the outer conductor of the sensor can change with the onset of a crack in the concrete in which it is embedded. For example, Fig. 1 shows the change of current flow path on the outer conductor of the sensor. When two spirals that are originally in perfect contact are partially separated, the original continuous cylindrical outer conductor at zero load becomes spiral at the location of partial separation, and, thus changes the topology of the sensor. This topological change results in a detour of the current path. Therefore, one of the most critical sensor parameters is the mechanism to allow partial separation of two adjacent spirals. In the case of rubber-sensors, the outer spirals were bonded with adhesive on the rubber tube and it was the flexibility of the rubber tube that enables the separation of spirals when subjected to a pair of equal but opposite forces (Chen, *et al.* 2004).

2.1. New design of sensors and their physical properties

The new design of crack sensors differs from the rubber-sensors in the use of dielectric material and the fabrication process of their outer conductor. The new sensor is made up of an inner conductor, a rigid dielectric material, and an outer conductor which is coated with a layer of solder as can be seen in Fig. 2. The inner conductor is made up of 10 gage twisted silver plated copper wires surrounded with a PTFE (Teflon) dielectric. As such, the sensor is herein referred to as a Teflon-sensor. The outer conductor of the sensor is a stainless steel spiral material. The inner conductor is 2.8 mm in diameter

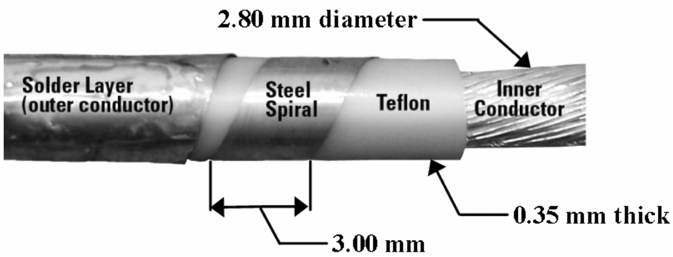

Fig. 2 Cut-away sample of a Teflon-sensor

and the dielectric material is 0.35 mm thick, while each turn of the spiral is 3.0 mm in width as shown in Fig. 2. The spiral is wrapped without adhesive around the dielectric in such a way as to ensure that each turn of the spiral is touching edge to edge without any gap or overlapping. The spiral can therefore slide along the dielectric. A thin coat of solder is then applied evenly over the entire surface of the spiral enabling the spiral to remain in place and allow for a continuous axial current path over the surface of the outer conductor at zero loading. The solder is strong enough to hold the spirals in place while still allowing for the spirals to separate when the concrete surrounding the sensor cracks and pulls the spirals apart. This enables the outer conductor to be electrically continuous but mechanically separate. The sensors are embedded in 1.27 cm×1.27 cm (½ in×½ in) channels in the face of RC members and grouted into the channel using a masonry grout. When the crack propagates across the channel containing the sensor, the grout also cracks with the member. The grout adheres to the outer conductor of the sensor and when the grout cracks, the spiral is separated.

2.2. Signal measurement

The measurement principle implemented in the crack detection system is electrical time-domain reflectometry (ETDR). This involves sending a pulse down a signal carrier, cable or sensor, and the reflection of that signal is then sampled. With a sampling device, time-domain reflectometer (TDR), a bandwidth of 20 GHz can be achieved for repetitive signals at a sampling rate of 200 kHz, using equivalent sampling techniques. If there is an impedance change or discontinuity at one location along the length of the cable, the reflection of the input signal at that location will be distinguishable from the remaining portion. This discontinuity is because of some type of change or interruption in the path of current. This is brought about by either a geometric change of the cable cross-section, or by a change in topology of one of the conductors. In the case of the distributed crack sensors in this study, the change in topology of the outer conductor is what causes an interruption of current flow at the location of a crack in the concrete, as illustrated in Fig. 1. When the crack in the concrete propagates across the sensor, the solder across the joint between the spirals at that location is broken and the spirals are pulled apart. This causes a change in the current path, resulting in a signal discontinuity and reflection in the sensor at that particular location. How much separation between spirals and how many spirals are pulled apart determines the amplitude of the reflected signal. It is in this way that the relative size of the

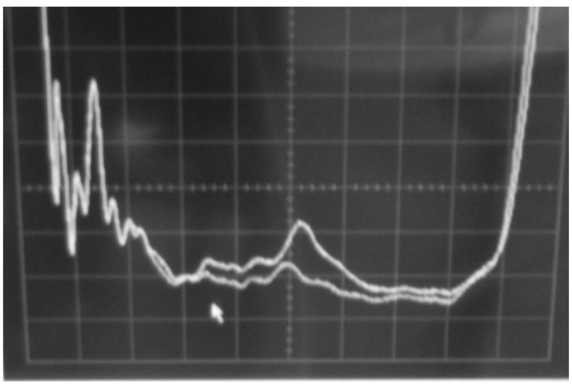

Fig. 3 Snapshot of TDR screen showing real-time signal from the sensor in Beam B5 under tension (top line) along with data captured before loading (bottom line)

crack can be determined by relating it to the amplitude of the reflected signal. Fig. 3 shows a typical sensor signal in real-time as seen on the screen of the TDR (top line only). The location of the discontinuity along the length of the sensor can also be determined from the delay time of the reflected wave. The signal on the sampling device shows the electrical equivalent of the sensor on the screen in time versus the reflection coefficient, which is a measure of how much of the signal is reflected. This reflection coefficient is directly related to the discontinuity in the sensor at the point of deformation (Chen, *et al*. 2004). Since the material properties of the sensor are known, the velocity of the signal can be determined and the time can be directly converted into length, which allows for correlation between the electrical location of the discontinuity and the physical location of the crack.

Before any cracking occurs, a baseline signal is recorded. This baseline is subtracted from all data taken during testing to get a better understanding of what changes are taking place in the sensor. Although the cracks that occur can easily be seen from the raw signal, taking out a baseline more clearly shows the change in the reflected signal at the onset of a crack.

3. Dynamic tests of columns with embedded sensors

3.1. Column specimen

A total of six RC column specimens were tested on the shake table in the high-bay structures lab at the University of Missouri-Rolla as illustrated in Fig. 4. The shake table has a payload capacity of 90 kN (20 kips). It operates effectively in a frequency range of 0.1~10 Hz with +/-2.54 cm (1 in) stroke. Fig. 5 shows the dimensions and reinforcement of the column specimen. Designed with 27.5 MPa (4 ksi) concrete and Grade 60 rebar, each specimen consisted of a footing, a column, and a mass of concrete cast into the top of the column. The footing contained No. 13 (#4 in English Unit) longitudinal reinforcement in both the top and bottom, which was confined by No. 10 (#3) stirrups spaced every 15.24 cm (6 in). The column was 20.32 cm (8 in) square in cross section and was 114.3 cm (45 in) in

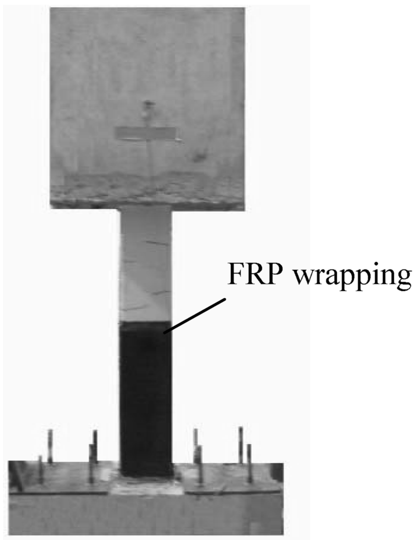

Fig. 4 Column specimen fastened to shake table

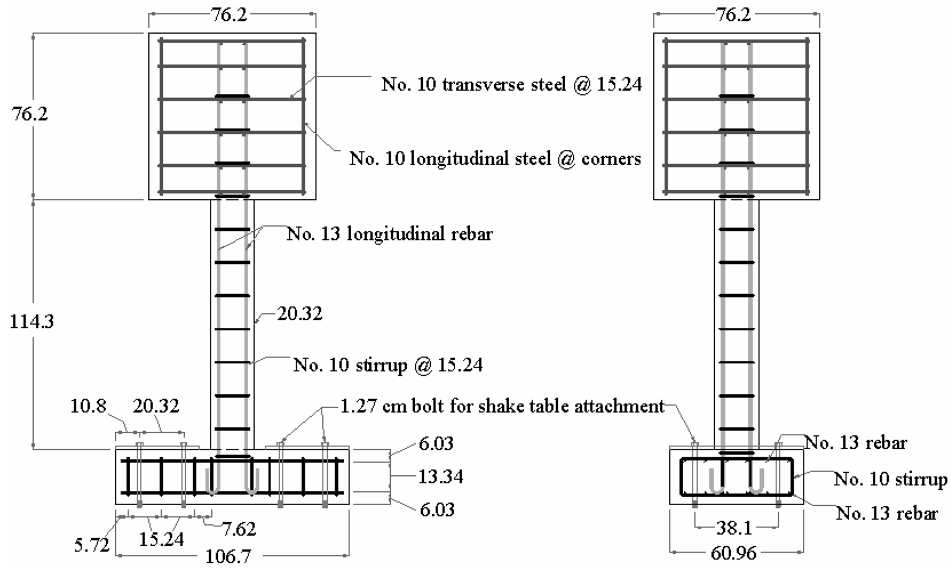

Fig. 5 Reinforcement detail of column specimen (all dimensions in cm)

height. The column reinforcement consisted of four No. 13 (#4) rebars confined by No. 10 (#3) stirrups spaced every 15.24 cm (6 in). The mass was cast into the top of the column to ensure that the natural frequency of the specimen was within the limit of the shake table or 10 Hz. The final design of the specimen allowed for a natural frequency before cracking on the order of 8 Hz.

3.2. Column test matrix and results

One sensor was installed in each square RC column that was tested under sinusoidal loading. The test matrix of six columns is presented in Table 1, with and without retrofitting using fiber reinforced polymer (FRP) composites for the purpose of illustrating both surface and hidden cracks. Each column was tested by incrementally increasing the excitation frequency from 2 Hz to 9 Hz and then back down to 2 Hz in order to obtain useful column response data around the natural frequency of the column. This was done at increasing stroke levels from 0.254 mm (0.01 in) to 3.81 mm (0.15 in). In general, the largest stroke level corresponds to fracturing of the vertical reinforcement at the column-footing interface after approximately 20,000 cycles of loading. During testing, it was often observed

Table 1 Test matrix of column specimens

Column	Retrofit	Stroke (mm)	Rubber-Sensor	Teflon-Sensor	Crack
C1	No	1.78	N/A	T1	Surface
C2	No	1.78	N/A	T2	Surface
C3	Yes	1.78	N/A	T3	Hidden
C4	Yes	1.78	N/A	T4	Hidden
C5	Yes	0.76	N/A	T5	Hidden
C6	No	0.76	R1	N/A	Surface

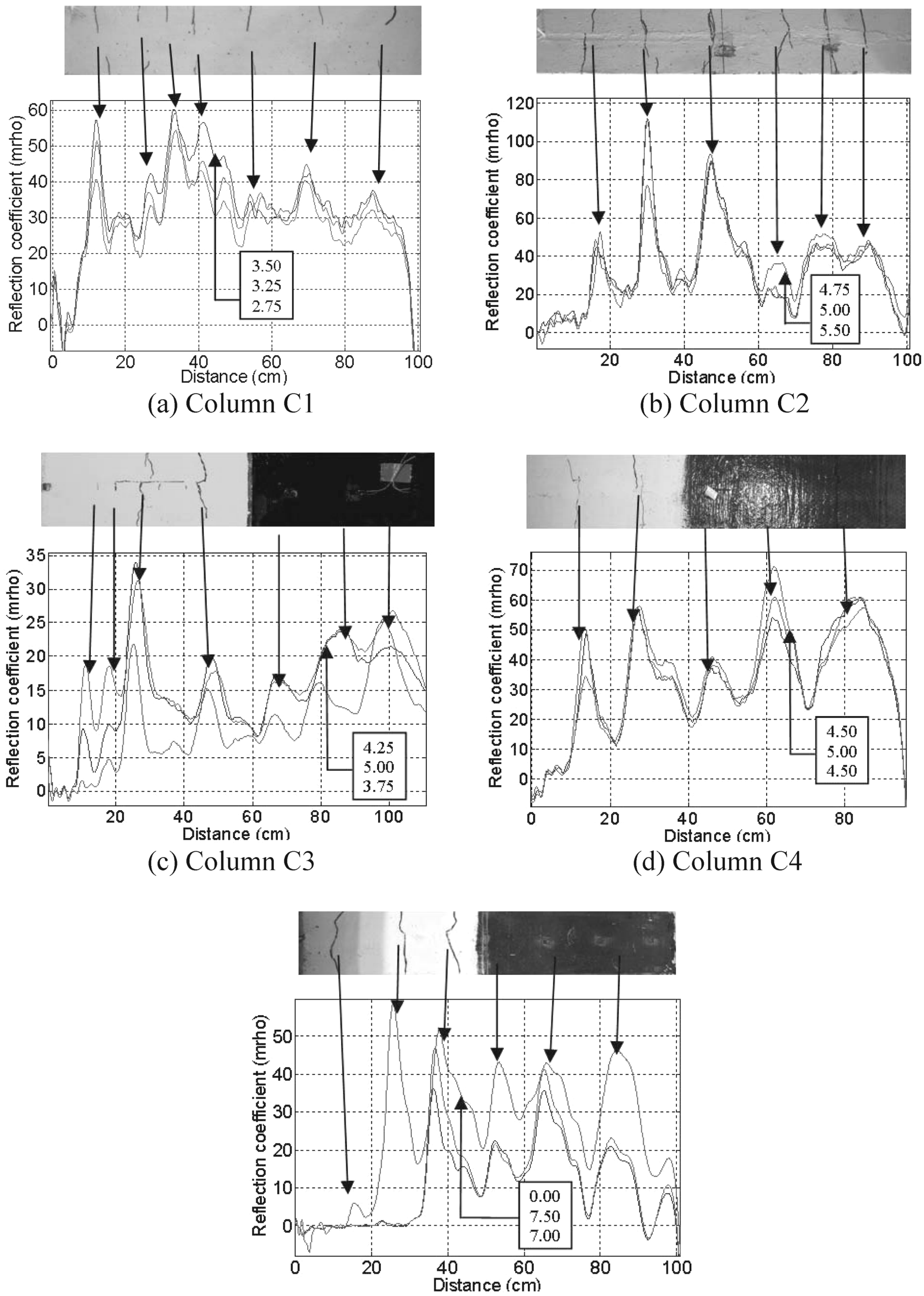

(a) Column C1 (b) Column C2 (c) Column C3 (d) Column C4 (e) Column C5

Fig. 6 Difference signals taken at given excitation frequencies in Hz (legend) that the signal from the TDR would reveal cracks in the column face before the cracks were observed by visual inspection. At the stroke specified in Table 1, the crack pattern on all columns and the corresponding TDR signal waveform (difference from the baseline prior to loading) are presented in Fig. 6. It is clearly seen from Fig. 6 that all cracks have been successfully identified with the measured signal. The data shown for Columns C1-C4 are at a table stroke level of 0.178 cm and the data for Column C5 was recorded at a stroke level of 0.076 cm. The decreasing levels represent data taken at the frequency shown in the legend in Hz. The reflection coefficient changes with the excitation frequency, representing the dynamic effect on the column behavior. In Columns C3-C5, FRP wrapping was applied to the lower 61 cm (24 in) of the column. The sensors were installed before the FRP was wrapped around the columns so that the ability of the sensors to detect cracks beneath such retrofit options, which would normally conceal cracks, could also be investigated. In Columns C3 and C4, fibers were oriented horizontally so that the cracks that had occurred beneath the FRP would separate the FRP sheets in the weak direction of the fibers and could therefore be seen at the surface of the FRP sheets. The sensors accurately detected the location of these cracks beneath the wrapping. In Column C5, the cracks beneath the FRP could not be physically seen because two FRP sheets had been applied with horizontally- and vertically-oriented fibers, respectively. However, Sensor T5 in that specimen did show that there were cracks across the face of the column in the retrofitted region as indicated in Fig. 6 for Column C5. It is clearly seen from Fig. 6 that the location of cracks in the signal correlates well with their respective physical locations at all excitation frequencies.

3.3. Teflon- versus rubber-sensors

To understand the performance of rubber-sensors under dynamic loading, one such sensor was installed in Column C6 as indicated in Table 1. At an excitation frequency of 5.00 Hz, 5.25 Hz, 5.50 Hz, and 7 Hz, respectively, the reflected signal from the rubber-sensor is shown in Fig. 7 at a stroke of 0.762 mm (0.03 in). In comparison with Fig. 6, Fig. 7 indicates that the reflected signal from the rubber-sensor is considerably smaller in responding to the occurrence of cracking. This is due in part to the fact that the rubber material likely delays its response to the rapidly cracking effect due to the material

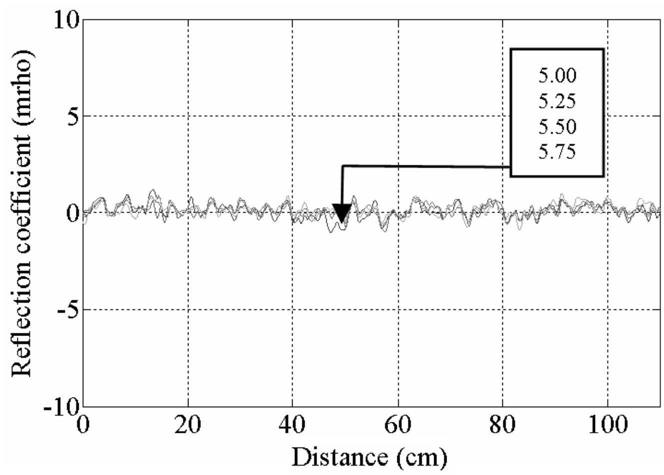

Fig. 7 Difference signal from Rubber-sensor R1 at given excitation frequencies in Hz (legend)

viscosity under dynamic loading. Therefore, the rubber-sensors are more applicable to slowly developed cracks or strain measurements as discussed in Chen, *et al*. (2004).

3.4. Data acquisition issues

For dynamic tests, it is critical to have a systematic procedure to acquire the time-varying signal from the sensors. With the commercially available Agilent Infiniium DCA Wide-Bandwidth Oscilloscope that was used in these tests, the data from the TDR signal could not be recorded continuously unless an interface between instruments and data acquisition, such as GPIB or IEEE-488 bus, has been installed. In this study, due to the equivalent sampling method, it only takes approximately 2.6 milliseconds for the reflected signal along the entire length of the sensor to be captured. This is not a problem, since the highest tested input frequency was on the order of 9 Hz. Therefore, each desired signal was saved manually during the tests. Every effort was made to capture the sensor's signal at the moment of maximum deflection, when the cracks would be opened to maximum width. This proved to be the difficult task of data acquisition. However, in nearly all cases, the signal was captured at or very near maximum deflection.

3.5. Sensor fatigue

Another issue that needed to be addressed with these new sensors is fatigue life. During the shake table tests, it has been observed that all sensors continued to be functional until the failure of tested columns (fracture of main reinforcement) after over 20,000 cycles of motion. The only unexpected situation was with a loose connector at the end of Sensor T1 that resulted from bending back and forth repeatedly during testing, but this connector was easily repaired. In the event that a sensor might be damaged, it would be relatively simple to cut the sensor from the groove and replace and re-grout a new sensor in its place without disturbing the structure itself. This is possible since the sensor was embedded into the face of the concrete usually no deeper than 1.27 cm (½ inch).

3.6. Discovery of memory feature

One of the more interesting discoveries after the dynamic column tests was the observation of the sensor being able to "remember" where the cracks had occurred after testing was completed. The peaks in the signal from the sensor corresponding to cracking remained visible in the signal once testing was complete, while it was difficult to detect the cracks on the face of the column visually. This can be very useful in post-disaster evaluation of RC structural members by more accurately and quickly ascertaining the damage that had occurred to the structure during the event. Fig. 8 shows the signal from Columns C4 and C5 captured after testing was complete. It can be seen from Fig. 8 that the cracks that had opened during motion are still visible in the sensor signal.

As will be discussed in Section 4, the observed feature above is actually a result of the occurrence of the permanent displacement or misalignment on the sensor. For lack of a better term, it is referred to as a "memory" feature in the remaining presentation. The memory feature will enable the sensors to be implemented either with or without a network for earthquake damage assessment. If a network is used, then it would be possible to acquire real-time data from the crack sensors. It is also possible to implement the sensors without a network, since data reflecting the important part of the crack history close to the maximum crack width can be obtained from the sensor after an event has taken place. This

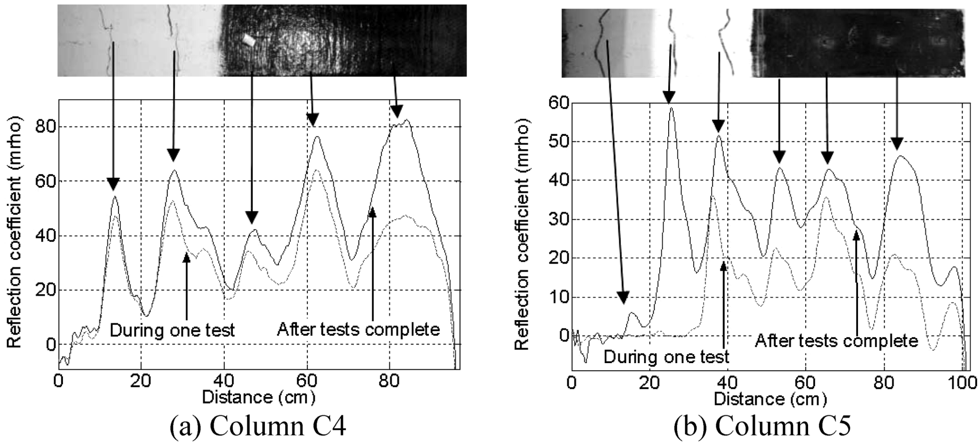

Fig. 8 Difference data captured during testing and memorized after tests were completed

is significant because it allows for useful data to be obtained in the event that data acquisition equipment either loses power or is damaged. This memory feature was investigated more closely and is discussed in the next section of this paper.

4. Memory feature characterization test

With the discovery of the memory feature, a new test protocol was developed to understand when the memory feature appears. The memory feature is related to the sliding mechanism of spirals over the dielectric of a Teflon-sensor. When the crack opens, the spirals are separated locally, and when the crack closes again, the spirals can be misaligned which will continue to reveal a discontinuity in the signal. A schematic representation of the misalignment is represented in Fig. 9. From this figure, one can see that the edges of the spirals are no longer in contact with one another after they have been pulled apart. Therefore the width of a crack, the rate of loading, and the number of times that the crack opened and closed are considered possible parameters contributing to the permanent deformation of the outer conductor of the sensor at the location of a crack.

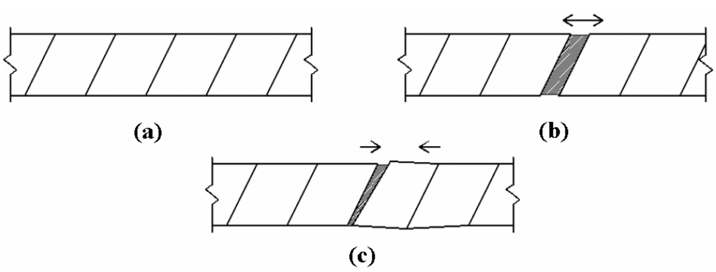

Fig. 9 Separation and resultant misalignment of spirals under dynamic loading

Table 2 Test matrix of beam specimens

Beam	Type	Sensor	Effect studied
B1	I	T6	No. of cycle
B2	I	T7	Crack width/No. of cycle
B3	II	T8	Crack width/No. of cycle
B4	II	T9	No. of cycle
B5	I	T10	Load rate
B6	II	T11	Load rate

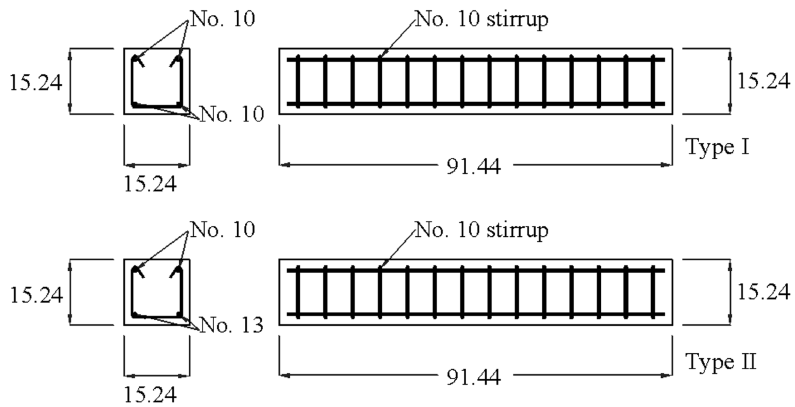

Fig. 10 Reinforcement detail of small-scale beam specimens (all dimensions in cm)

4.1. Test specimen and setup

A total of six small-scale RC beam specimens were tested under static and cyclic loading as described in Table 2. Each beam was 15.24 cm (6 in) square in cross section and 91.44 cm (3 feet) in length, as shown in Fig. 10, and were constructed of 27.5 MPa (4 ksi) concrete. All were doubly reinforced; two had No. 10 (#3) reinforcing bars in the tension face (type I), while the other two had No. 13 (#4) reinforcing bars in the tension face (type II). Both had No. 10 (#3) stirrups spaced at 6.35 cm (2.5 in) with the compression reinforcement for both types consisting of No. 10 (#3) rebar. A reinforcement schedule for the two types of beams is also given in Fig. 10.

One Teflon-sensor was installed in the tension face of each beam by 1.27 cm (1/2 in) deep in the groove as illustrated in Fig. 11(a). Each beam was tested under a three-point loading system as shown in Fig. 11(b). The beam was simply supported 7.62 cm (3 in) from each end and the load was applied at the center point (mid-span) of the top of the beam through a roller bearing. This series of tests were conducted in three phases. The purpose of the first phase of the experiment was to correlate crack width to the change in the reflected signal with static tests, and to understand the effect of crack width on the memory feature. The second phase was intended to ascertain how many cycles it would take to develop a crack memory with cyclic tests. The last phase was designed to understand the effect of loading rate with additional cyclic tests.

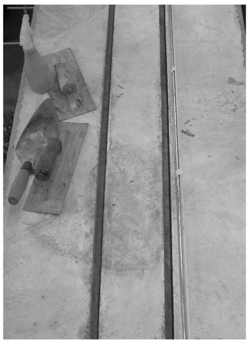

(a) Example of grooves for sensor installation at the tension face of the beam

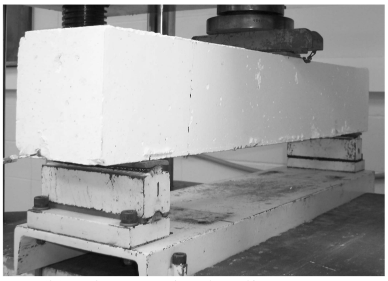

(b) Three-point loading test setup

Fig. 11 Small-scale RC beam and cable sensor installation

4.2. Test procedure

For the static loading case, the beam was loaded in incrementally increasing levels so that as cracks appeared, their width could be physically measured at each loading level to compare with the reflected signal from the sensor. The loading was displacement controlled with the Tinius Olsen machine so that the width of the cracks would remain as constant as possible while measuring was taking place. As the cracks started to propagate, their width would be measured with a crack scope with a resolution of 0.025 mm (0.00098 in) and a maximum measurable width of 3 mm (0.12 in). The loading displacement level was measured at the mid-span of the beam and was typically increased in steps of 0.5 mm (0.02 in), however, in some cases when it was observed that the signal from the sensor at the location of a crack was changing rapidly, that interval would be decreased to 0.25 mm (0.01 in) so that the progressive opening of the cracks could be captured in better detail with additional data points. The load deflection was increased until the beam was near the point of yielding based on the change in slope of the load-displacement curve.

For cyclic tests with the Tinius Olsen machine, a constant deflection was repeated throughout an increasing number of cycles. Each beam was loaded to a maximum deflection of 80% of its maximum deflection from the static tests. The deflection value was chosen so that the cracks would open significantly yet preventing the beams from yielding or failing. The load was applied and then released at a rate of 0.762 mm/sec (0.03 in/sec) which was limited by the loading machine. Data was recorded from the sensor at peak displacement and then again after each set of cycles was complete, at no load, to capture the memory phenomenon. The beams were tested until it was observed that there was very little or no change in the reflected signal from the TDR at each crack location in the unloaded condition.

To see the effect of a higher loading rate on memory feature, two additional beams (B5 and B6 in Table 2) were cyclically tested. In these cases, a small groove, 3.2 mm in depth (0.125 in) was cut in the bottom center of the beams to control the location of the largest crack. Both beams were first loaded statically with the Tinius Olsen machine until the first crack was discernable in the signal and visible by sight. Beam B5 and Beam B6 were subjected to a mid-span deflection of 2.54 mm (0.1 in) and 3.81 mm (0.15 in), respectively, due to their difference in reinforcement. Once the data from this setup was recorded, the specimens were placed in the MTS880 loading machine and loaded with half-sine motion at a frequency of 1 Hz, or 7.62 mm/sec (0.3 in/sec), in 5 cycle increments. At the end of each 5-cycle set, data was recorded from the crack sensors at zero loading.

4.3. Crack width versus reflection coefficient

Fig. 12 shows the reflected waveform at different loading levels, and the crack pattern corresponding

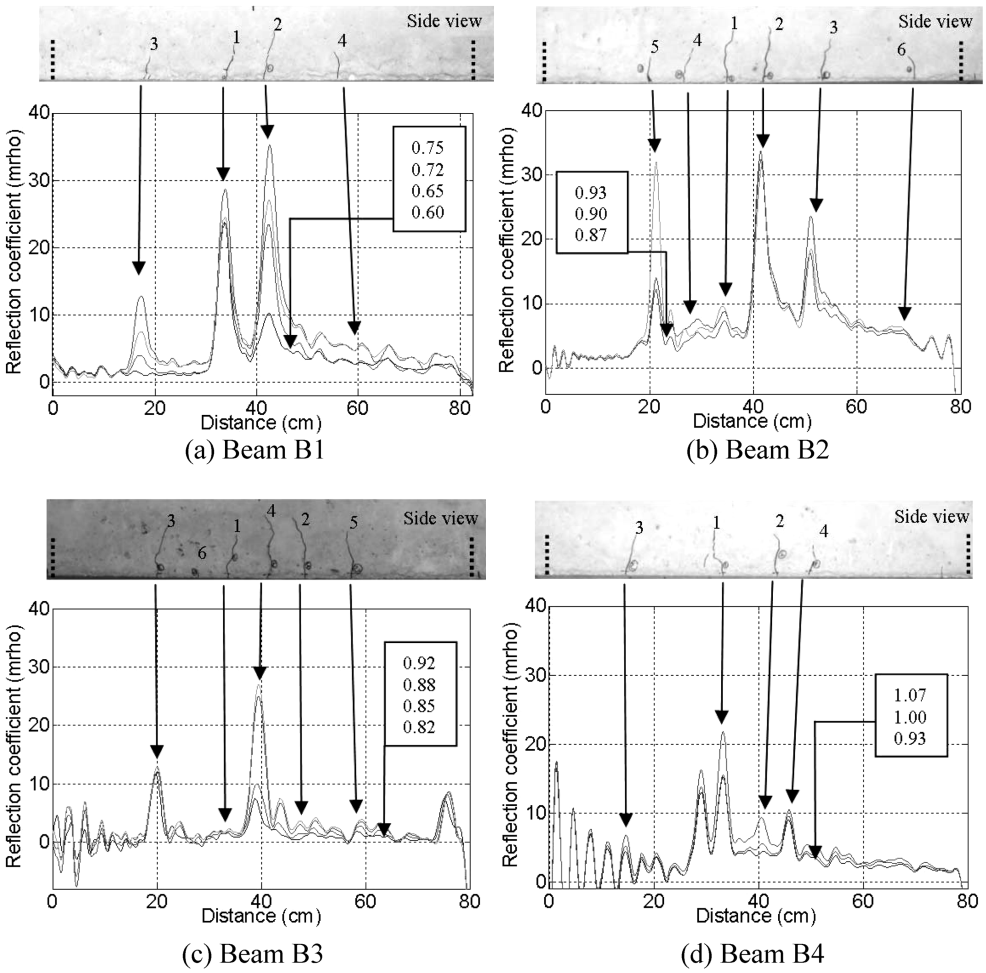

Fig. 12 Difference signal captured at mid-span deflection levels in percentage of span length (legend) with the start and end of the sensor represented by dotted lines

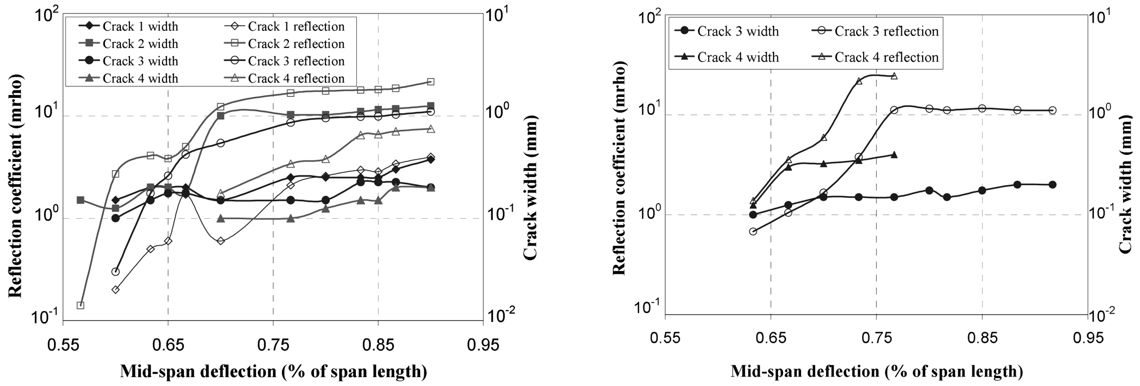

(a) Beam B2 (b) Beam B3

Fig. 13 Change in reflection coefficient at crack location and corresponding crack width vs. mid-span deflection expressed in percentage of span length

to the largest static load for Beams B1-B4. It was observed from Fig. 12 that the smallest crack that would be detectable according to the data recorded from the crack sensors was typically around 0.15 mm (0.006 in). This value of crack width is larger than that observed in the previous study (Chen *et al*. 2004), which is attributable to the application of soldering outside the steel spirals. Even so, this is still within the desired detectable range for structural applications (Nawy 2003). Fig. 12 also indicates that the location of most cracks can be clearly identified from the measured reflection coefficient. It is noted that some of the cracks shown on the side view of beams may not actually pass through the sensor installed at the bottom face of the beams. This may explain why a few cracks seem missing from the measured signals.

An attempt was made to quantify the relationship between increase in crack width and increase in change of the reflected TDR signal from the sensor data. Fig. 13 shows both the reflection coefficient and crack width of Beams B2 and B3 under various loading conditions that are represented by the midspan deflection in terms of percentage (%) of the span length. The crack number shown in Fig. 13 refers to Fig. 12. In general, the results show an increase in reflection coefficient as the crack width increases, especially at low loads. For each particular crack, the curves for reflection coefficient and crack width show an excellent trend for correlation. It is observed from Fig. 13 that at a load level of approximately 0.70%, the crack width and the reflection coefficient corresponding to crack 1 of Beam B2 drops steeply. This can be explained by the dramatic widening of the adjacent crack, crack 2, at that loading level, resulting in stress redistribution of the beam. The curves corresponding to crack 1 begin to increase again as the loading level increases. The presence of multiple cracks makes it difficult to establish a representative correlation between the reflection coefficient and crack width. It is noted that, in Fig. 12(d), several peaks were shown in the reflection waveform of Beam B4 between zero and approximately 15 cm due to loose contact of the end connection with TDR. This problem was identified during the testing and corrected before cyclic tests.

4.4. Effect of crack width on memory feature

At the end of static tests of Beams B2 and B3, the reflected waveform was acquired again after the loads applied on them had been removed. This time, only the largest cracks (>0.25 mm) could be seen

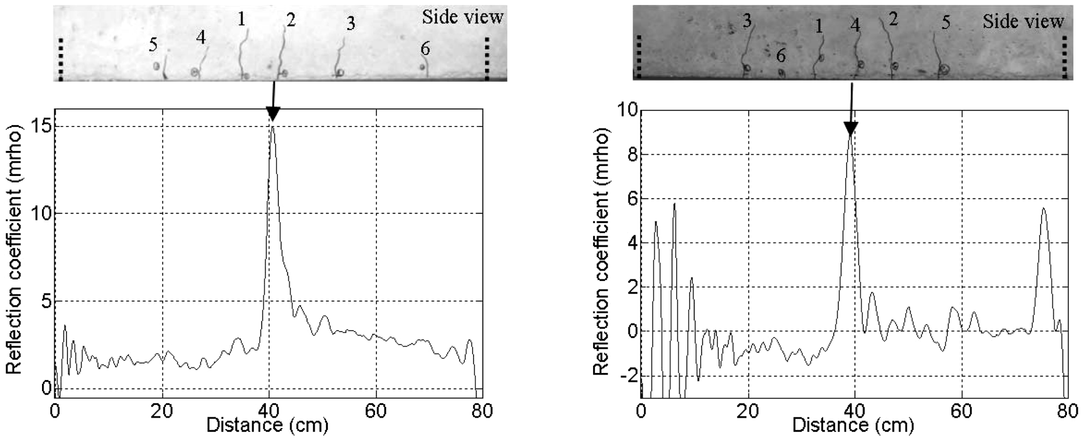

(a) Beam B2 (b) Beam B3

Fig. 14 Difference signal taken at zero load after static tests were complete with the start and end of the sensor represented by dotted lines

in the signal as shown in Fig. 14. This indicates that crack width is an important parameter affecting the memory feature. Even if a large crack opens only one time, the crack-induced separation of the spirals of the sensor outer conductor could be so large that misalignment of the spirals likely occurs when the crack closes. As illustrated in Fig. 1, this misalignment will cause a discontinuity in the current flow through the outer conductor of the sensor resulting in a permanent change in the reflected signal at that location. However, if the crack is small when it is opened, the spirals of the sensor outer conductor can return to their original configuration allowing for the current path to be undisturbed and no discontinuity to be seen in the signal. It is noted that Fig. 14(b) indicates some fluctuation of the reflected signal within approximately 15 cm due to loose contact of the end connection with the TDR device that was found and tightened immediately after that test.

4.4. Effect of the number of loading cyclic on memory feature

Even though a crack is relatively small, when the spirals are separated a number of times due to opening and closing of the crack, some fatiguing of the spiral material likely takes place, and due to permanent deformation, the spirals will again remain misaligned creating a discontinuity in the sensor. As shown in Fig. 14, the largest crack in Beams B2 and B3 remained in memory after only one cycle of loading. In each case the rest of the cracks remained visible in the signal at no load after no more than 15 cycles as shown in Fig. 15. The peaks corresponding to each crack grew in magnitude of reflection coefficient as the number of cycles increased. However, typically by 160 cycles, the peaks had stabilized. These observations confirm that the smaller cracks do in fact remain detectable in the signal at no load after a very low number of cycles. It can be seen from Fig. 15 that the crack pattern in each beam was consistent. In each instance, the cracks near the center of the beam were the largest in width. The cracks that opened away from the center were smaller in magnitude. It can be seen that as the number of cycles increase, the magnitude of the disturbances in the reflected wave become larger. This figure also shows the excellent correlation of the location of major cracks along the beams.

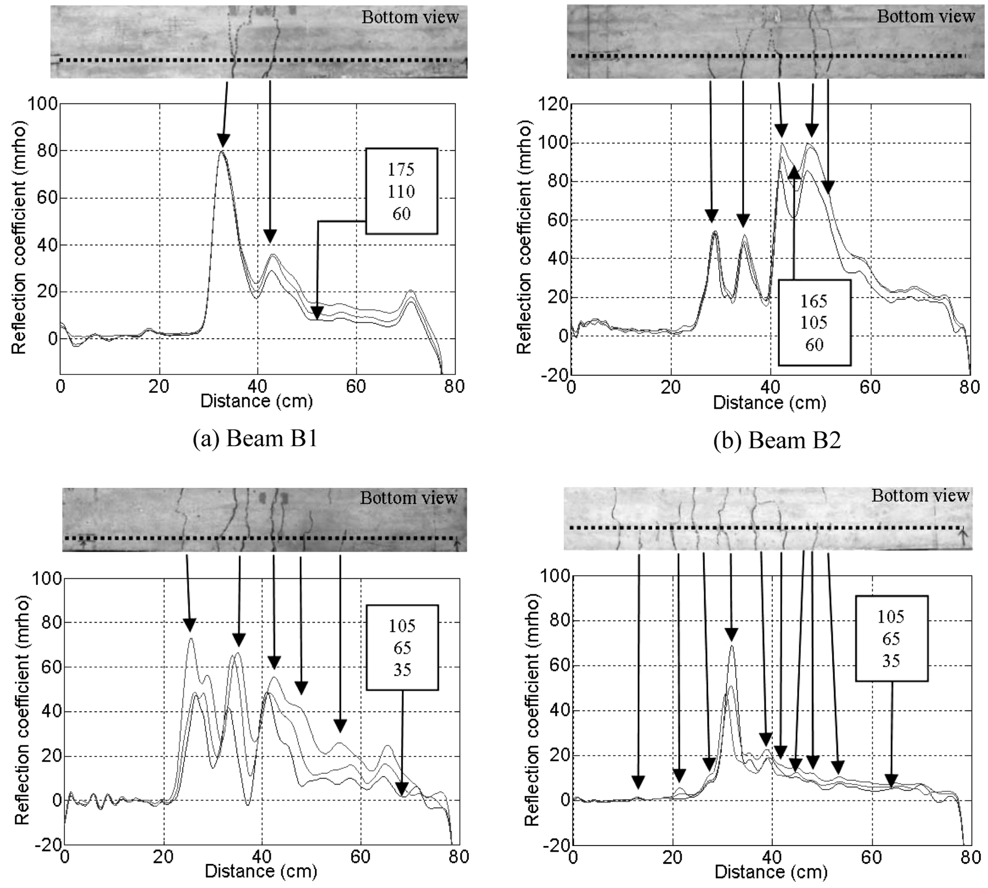

(a) Beam B1 (b) Beam B2

(c) Beam B3 (d) Beam B4

Fig. 15 Difference signal captured at zero load after given number of cycles (legend) with the location of the sensor shown in dotted lines

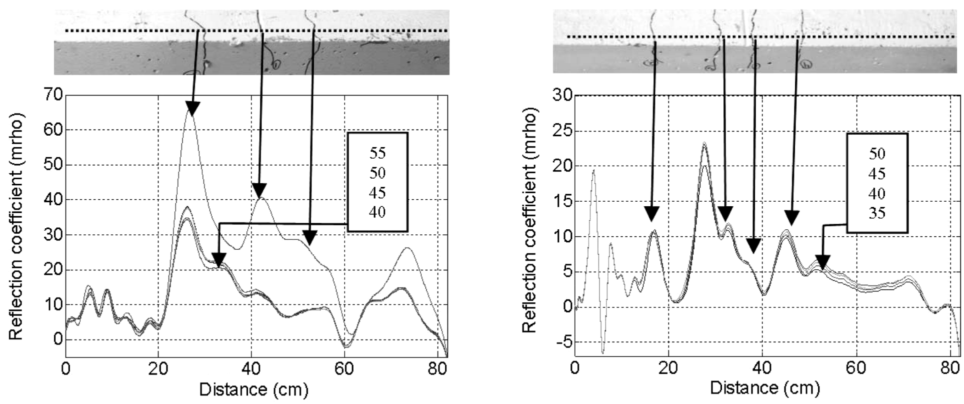

(a) Beam B5 (b) Beam B6

Fig. 16 Difference signal captured from sensor at zero load after given number of cycles (legend) with the location of the sensor shown in dotted lines

While the majority of the cracks are apparent in the signal from the sensor at zero load, some of the smallest cracks do not show up even after several cycles. This is further reason for the implementation of a method of data acquisition that will capture a time-history of crack data. This will further improve the performance of the crack sensor system enabling the detection of all cracks that are sufficiently large to have structural implications.

4.5. Effect of loading rate on memory feature

The results from the cyclic tests of Beams B5 and B6 are presented in Fig. 16. They are consistent with those from the cyclic tests of Beams B1-B4 under slower loading in that the number of cycles required to invoke the memory of the sensor were in the same order. Within the first five cycles of loading the largest crack was visible in the signal at zero load. More cracks propagated within the first five cycles as well. The width of those cracks were not able to be physically measured with the crack scope due to the test setup, however, they were smaller in size than the initial crack in both cases and were similar in size and in pattern to the cracks in Beams B1-B4. The smaller cracks from the previous tests began to remain in the signal at zero loading within 15 cycles. Fig. 16 shows how the cracks began to become increasingly visible as the number of cycles increased. It can also be seen from the photographs that, once again, location of the cracks are easily determined from the crack sensor signal.

5. Conclusions

The dynamic performance of distributed crack sensors has been studied through the shake table tests of six RC columns. After the discovery of the memory feature of the sensors, an attempt was made to quantify the memory feature with a series of static and cyclic tests of six RC beams. Based on the experiments, the following conclusions can be drawn:

1. The newly-designed, Teflon-sensors have performed well under static and dynamic loads while the rubber-sensors are more suitable for structures subjected to static loads. Both sensors proved to be rugged and durable. In the shake table column testing application, both sensors survived over 20,000 cycles of loading without failure. In the crack width calibration and cyclic testing, the Teflon-sensors encountered numerous relatively large cracks and did not show any signs of failing.

2. For a particular crack, the increase in crack width was in general agreement with the increase in reflection coefficient at the crack location. However, the relationship between physical width and resulting change in reflected signal is not consistent throughout the number of cracks due to multiple crack effects on stress redistribution, unknown sensor-concrete interaction, and adhesion. It was observed that the smallest crack width that is discernable according to the sensor is approximately 0.15 mm (0.006 in). Although larger than that of the sensors without soldering on spirals, this value is much smaller than the smallest crack width of structural implications.

3. In almost all test cases, the location of cracks can be clearly identified from the measured signal when the cracks open. Even after the load has been removed, large cracks (> 0.225 mm) can remain permanently discernable in the sensor signal while small cracks (< 0.20 mm) remain detectable in the signal typically after no more than 15 cycles of loading. The memory feature depends on both crack width and the number of loading cycles; it is independent of the load rate within the test range of up to 7.62 mm/sec (0.3 in/sec).

4. For cyclic testing, the Agilent Infiniium DCA Wide-Bandwidth Oscilloscope is sufficient for the

acquisition of reflection waveforms at any time. Even for harmonic/dynamic testing in the frequency range of 1-9 Hz, though somewhat challenging, the capturing of data at the moment of maximum crack width proved to be achievable. In both cases, the signal from the sensor on the TDR screen changes in real time as the cracks opened and closed. This observation reveals the possibility for future data acquisition techniques using a TDR sampling device with a GPIB interface card that will enable a time-history of crack propagation to be captured.

5. To improve upon the lower limit of detectable crack width and the correlation between reflected signal and crack width, further research in three areas are necessary: a) use of an automatic spray metallization process, b) understanding of the concrete-to-sensor interfacial and adhesion behavior, and c) controlled cyclic testing of beams with a progressively increasing single crack.

Acknowledgements

Financial support to complete this study was provided in part by the National Science Foundation under award number CMS0200381 and CMS9733123, the United States Department of Transportation, and the University Transportation Center at the University of Missouri-Rolla. The findings, results, and opinions expressed in this paper are those of the authors only and do not necessarily represent those of the sponsors. Thanks are extended to Mr. Xi Huang and Mr. Chris Courtright, graduate students, for their assistance during the shake table tests.

References

Benson, C. H. and Bosscher, P. J. (1999), “Time-domain reflectometry (TDR) in geotechnics: a review”, *Nondestructive and Automated Testing for Soil and Rock Properties*. ASTM STP 1350, W.A. Marr and C.E. Fairhurst, Eds, American Society for Testing and Materials, West Conshohocken.

Chen, G. D., Sun, S. S., Shen, X. L., Pommerenke, D., Greene, G. G., Belarbi, A., and Mu, H. M. (2003), “Crack detection of a 15 meter long reinforced concrete girder with a single distributed cable sensor”, *Proceedings of 1st International Conference on Structural Health Monitoring and Intelligent Infrastructures*, Tokyo, Japan, November.

Chen, G. D. (2004), “Development and validation of novel distributed coaxial cable sensors for crack detection”, *Proceedings of 3rd Sino-Japan-US Symposium on Structural Health Monitoring and Control*, Dalian, China, October.

Chen, G. D., Mu, H. M., Pommerenke, D., and Drewniak, J. L. (2004), “Damage detection of reinforced concrete beams with novel distributed crack/strain sensors”, *J Struct. Health Monitoring*, to appear.

Lin, M. W., Abatan, A. O., and Zhang, W. (1998), “Crack damage detection of concrete structures using distributed electrical time domain reflectometry (ETDR) sensors”, *Proceedings of 5th SPIE Annual Symposium on Smart Structures and Materials: Smart Systems for Bridges, Structures, and Highways*, Vol. 3325, Newport Beach.

Lin, M. W., Abatan, A. O., and Zhou, Y. (2000), “High sensitivity electric TDR distributed strain sensor”, *Proceedings of 7th SPIE Annual Symposium on Smart Structures and Materials 2000: Smart Systems for Bridges, Structures, and Highways*, Vol. 3986, Newport Beach, March.

Nawy, E. G. (2003), *Reinforced Concrete: a Fundamental Approach*, 5th Edition, Prentice Hall, Upper Saddle River, NJ.

O’Connor, K. M. and Dowding, C. H. (1999), *Geomeasurements by Pulsing TDR Cables and Probes*, CRC Press.

Su, M. (1997), “Quantification of cable deformation with time domain reflectometry techniques”, Ph.D. Dissertation, Northwestern University, Evansville.

Sun, S. S., Pommerenke, D., Drewniak, J. L., and Chen, G. D. (2004), “Signal loss, spatial resolution, and sensitivity of long coaxial crack sensors”, *Proceedings of 11th SPIE Annual Symposium on Smart Structures and Materials*, San Diego, March.

CC